Desalination and Water Treatment
www.deswater.com

doi: 10.5004/dwt.2019.24515

166 (2019) 353–364
October

Removal of copper(II) ions from wastewater using HA-coated-limestone

Dan Li[a], Wenjin Chen[a], Guigen Zhou[b], Feigao Xu[b,*]

[a]*School of Resources, Environmental and Chemical Engineering, Nanchang University, 999 Xuefu Avenue, Nanchang 330031, China, Tel. +86 791 86763662; email: 13122568@qq.com (D. Li), 892574504@qq.com (W. Chen)*
[b]*College of Chemistry, Nanchang University, 999 Xuefu Avenue, Nanchang 330031, China, Tel./Fax: +86 791 86763662; emails: xufeigao@ncu.edu.cn (F. Xu), 443883103@qq.com (G. Zhou)*

Received 3 January 2019; Accepted 9 June 2019

ABSTRACT

In this study, hydroxyapatite (HAp)-coated-limestone was prepared using waste limestone and diammonium hydrogen phosphate. Some factors have been investigated affecting the uptake behavior, such as phosphate addition times, preparation time, contact time, pH, temperature and copper ion concentration to optimize the conditions for maximum adsorption. Kinetic model, adsorption isotherm and thermodynamic parameters such as entropy change, enthalpy change and Gibbs free energy were calculated. The results showed that the adsorption capacity of HAp-coated-limestone is gradually increasing with the increase of phosphate addition times. The adsorption capacity of HAp-coated-limestone (1D + 1P, 2D + 2P, 3D + 3P, 4D + 4P) was 68.6, 72.1, 83.5 and 92.4 mg/g at 60 min, respectively. Adsorption process of copper ions on HAp-coated-limestone is in accordance with the second-order adsorption mechanics, and the adsorption isotherm indicated that the adsorption model was close to the Langmuir model. Thermodynamic parameters showed that adsorption process is spontaneous and endothermic. Both crystal form and coverage of limestone affected the specific surface of HAp-coated-limestone. Besides, the preparation cost was low and performance of adsorption was good.

Keywords: Copper; Removal; Adsorption; HAp-coated-limestone

1. Introduction

Because diseases caused by water pollution are difficult to cure, heavy metal pollution in water resources is increasingly valued by the people from all over the world [1]. Many heavy metals such as chromium, lead, copper and manganese are highly biologically harmful because of their acute toxicity, irreversibility, non-decomposability and bioaccumulation [2]. These heavy metals and their compounds can accumulate in humans and animals, along the biological chain, posing a serious threat to human and animal health, especially the circulatory system, the nervous system and the immune system. Human and animal adipose tissue and liver are very sensitive to the accumulation of heavy metals and may even develop cancer [3,4].

Copper is one of the trace elements that affect human health. And copper is a metal that is very close to human beings. With the development of pharmaceutical production, printing, metallurgy, electronics industry, a large number of copper-containing wastewater was discharged into nature, causing harm to people and environment [5]. Copper is actually necessary for human life, but excessive copper is harmful to people, animals and plants. Copper is very toxic to aquatic organisms, and also pernicious to human. In some rivers, there have been cases of poisoning from copper pollution. Excessive intake of copper ions can cause nausea, vomiting, diarrhea and even hematuria, jaundice, mental illness and serious death [6]. Therefore, it is important to treat the copper-containing wastewater to reduce the copper ion content to the allowable emission

* Corresponding author.

concentration. The maximum allowable levels of copper in drinking water in the World Health Organization and the US Environmental Protection Agency standards are 2.0 and 1.3 mg/L [7]. In addition, to achieve energy-saving environmental treatment of wastewater, the effective way to remove copper ions should be studied. A compound of copper exists at one or two valence states and Cu(II) is more harmful than Cu(I) in the wastewater environment [8]. Therefore, this research mainly studies the removal of Cu(II).

At present, the main methods of treating copper-containing wastewater are ion exchange [9], chemical precipitation [10], electrolysis [11], membrane separation [7], adsorption [12], etc. But most of these technologies have a higher demand for equipment, high cost and prone to secondary pollution [13]. Adsorption has the characteristics of low cost, simple and easy to handle without causing large environmental pollution. Adsorption method to treat copper containing wastewater has many advantages and becomes the focus of water treatment research. A lot of excellent adsorbents have been developed. Nowadays, adsorption has been shown to be the most effective way to remove heavy metal ions [14,15]. Commonly adsorbents used to remove copper ions adsorbent are activated carbon [16], carbon nanotubes [17], hydroxyapatite (HAp) [18], humic acid [19], titanium dioxide [20], etc. However, adsorption efficiency of many adsorbents is low and these adsorbents have a high cost, making some of the application of adsorbents limited [2]. The HAp is one of the components of bone, commonly used as a biological material [21], is also a copper ion adsorbent that is commonly used. HAp can be made easily with low cost. In addition, HAp has the characteristics of high adsorption efficiency, low cost, large specific surface area, good stability, but poor mechanical properties [22].

So far, many scholars have studied the adsorption properties of HAp, and found some methods to enhance the adsorption capacity of HAp. One of the methods is to increase the specific surface area of HAp, thereby increasing the number of binding sites with heavy metal ions. Increasing the specific surface area is usually achieved by reducing the size of the HAp, such as nano-HAp [23]. Compared with the HAp with a general size, its copper ion adsorption capacity is enhanced. However, nano-HAp has a drawback that it has a high osmotic pressure in the solution and is easy to copolymerize. A potentially alternative approach is to make use of the strong Cu^{2+} sorption capabilities of HAp and generate reactive nano- to micrometer sized HAp on submillimeter sized particles limestone. Kanno et al. [24] have prepared HAp-coated-limestone with limestone and sodium dihydrogen phosphate. Limestone provides an ideal reactive substrate because PO_4^{3-} interacts strongly with limestone surfaces. In addition, it is also a readily available, less expensive source of Ca^{2+} for HAp synthesis in the presence of externally added phosphate. Our previous study found that addition of ethanol (3 vol%) to the diammonium hydrogen phosphate remarkably increases F^- removal of the HAp-coated-limestone [25]. Most of these studies focused on the removal of F^-, with few studies on the removal of heavy metal. It had been demonstrated that the adsorption of F^- on the HAp-coated-limestone was mainly attributed to adsorption and ion exchange. Therefore, we speculated that the HAp-coated-limestone could also be used as an efficient adsorbent for the removal of Cu^{2+}.

The main objectives of this work are (1) to investigate how the diammonium phosphate addition times affects the surface topography of HAp-coated-limestone; (2) and to make sure whether there is a positive or negative correlation exists between phosphate addition times and removal of Cu(II); (3) to evaluate whether HAp-coated-limestone is suitable for the removal of Cu(II)-containing wastewater. With the help of bath adsorption experiments, effect of reaction time, initial Cu(II) concentration and addition times of phosphate on the adsorption quantity of HAp-coated-limestone was investigated. In addition, adsorption kinetics of HAp-coated-limestone was also investigated.

2. Materials and methods

2.1. Materials and reagents

Dihydrogen phosphate diamine was purchased from Sinopharm Chemical Reagent Corporation (Shanghai, China). Commercial HAp (particle size: 0–100 nm) and dicyclohexanoneoxaly dihydrazone was purchased from Shanghai Aladdin Company (Shanghai, China). All Cu^{2+} solutions were prepared from copper sulfate pentahydrate stock solution (J&K Group Chemical Reagent Co. Ltd., Shanghai, China). The sample limestone from Nanjing Dou village is composed of calcite (approximately 97%), with trace amounts of quartz, alumina and iron oxides. Limestone was crushed and screened to 75–150 micrometers. All water used was deionized.

2.2. Preparation of HAp-coated-limestone

HAp-coated-limestone was prepared as follows: 2.5 g limestone was added into 100 mL and 0.05 g/mL dihydrogen phosphate diamine at 800 pm and at 40°C. The reaction HAp happened based on the equation [26]:

$$10CaCO_3 + 5\left(NH_4\right)_2 HPO_4 \rightarrow Ca_{10}\left(PO_4, CO_3\right)_6\left(OH, CO_3\right)_2 + 5\left(NH_4\right)_2 CO_3 + 3CO_2 + 2H_2O \quad (1)$$

where PO_4^{3-} and OH^- can be partially replaced by CO_3^{2-}.

After 24 h of reaction, a small amount of reaction product was collected, filtered, washed with deionized water, and air-dried for microscopic analysis. Then, the reaction product was added into 0.05 g/mL dihydrogen phosphate diamine solution again and continued to react for 24 h. The whole reaction continued for 1–4 d. Four of them replaced the diammonium phosphate every day and were, respectively, reacting for 1, 2, 3 and 4 d. They were separately numbered 1D + 1P, 2D + 2P, 3D + 3P and 4D + 4P. The total of four samples is listed as Table 1.

2.3. Adsorption experimental

The batch experiments were conducted as follows: the equilibrium adsorption experiments were performed by adding 10 mg adsorbent into 100 mL Cu^{2+} solution (10, 15, 20, 25, 30 mg/L) at pH 6.8 and a certain temperature (303, 313, 323 K). A certain amount of adsorbed copper ion solution was

Table 1
Description of four types samples in this study

Sample name	Preparation temperature (°C)	Preparation time (d)	PO_4^{3-} addition times
1D + 1P	313	1	1
2D + 2P	313	2	2
3D + 3P	313	3	3
4D + 4P	313	4	4

removed at a certain time interval (5, 10, 20, 30, 40, 50, 60, 70 min). The maximum wavelength of Cu^{2+} was tested by the ultraviolet and visible spectrophotometer (purchased from Shanghai Mapada Instrument Co., Shanghai, China) varying from 300 to 750 nm. The adsorption capacity (Q_t) of HAp-coated-limestone was as follows:

$$Q_t = \frac{C_0 - C_t}{W} V \quad (2)$$

where C_0 (mg/L) is the initial concentration of copper ions, C_t (mg/L) is the concentration of copper ions after t min adsorption, W(g) is the weight of HAp-coated-limestone, V (L) is the volume of the copper ion solution used for adsorption. Q_t (mg/g) is the adsorption capacity of HAp on copper ions at time t.

2.4. Characterization of absorbent

Powder X-ray diffraction (XRD) patterns were obtained using Bede D1 system diffractometer with Cu Kα radiation (λ = 0.154 nm) in the 2θ range from 10° to 80° with a scan rate of 3 deg min^{-1}. The accelerating voltage and the applied current were 35 kV and 30 mA, respectively.

The chemical bonds of the synthesized materials were analyzed by Fourier transform infrared spectrophotometry (FTIR). The spectra of powders extracted from the samples were recorded using a Nicolet Nexus 5700 FTIR spectrometer in the region from 4,000 to 400 cm^{-1}.

The thermal behavior of samples was analyzed by using simultaneous differential thermal analysis (TA-SDT600), with a heating rate of 10°C min^{-1}–800°C min^{-1}. The instrument was purged with N_2 at a flow rate of 100 mL min^{-1}.

The textural properties of HAp-coated-stone samples were characterized by N_2 adsorption–desorption isotherms at 77 K in an automatic adsorption apparatus (ASAP2010; Micromeritics, USA). The samples were outgassed under high vacuum condition for 5 h at 200°C. The specific surface area was calculated with the BET method. The total pore volume was obtained from the amount of vapor adsorbed at a relative pressure (P/P_0) close to unity, where P and P_0 are the measured and equilibrium pressures, respectively. The pore size distributions were evaluated according to the desorption curves of the isotherms using the Barrett–Joyner–Halenda method.

A palladium-gold alloy was vacuum evaporated onto HAp-coated-limestone. Then the outer surfaces of these samples were, respectively, studied using a ZEISS EVO18 (Jena, Germany) scanning electronic microscope (SEM) at 3 kV of accelerating voltage under various magnifications.

3. Results and discussion

3.1. Characterization of HAp-coated-limestone

Fig. 1 reveals the infrared spectra of HAp-coated-limestone. It can be seen clearly that the absorption peaks of the four sets of spectra are almost identical, except the intensity and peak area are different. The bands at 1,102; 1,027 and 575 cm^{-1} represent the vibration mode of the tetrahedral PO_4^{3-} [27]. The characteristic absorption peaks of CO_3^{2-} groups is at 728, 874, 1,437 cm^{-1} [28]. The stretching vibration of the OH^- appears in the wavelength at 3,443, 2,530 and 1,820 cm^{-1}.

Thermal behaviors of HAp-coated-limestone and HAp are shown in Fig. 2. The results show three regions of interest in the TG curve: (1) The mass loss from 100°C to 200°C for all samples is due to the evaporation of water in the samples.

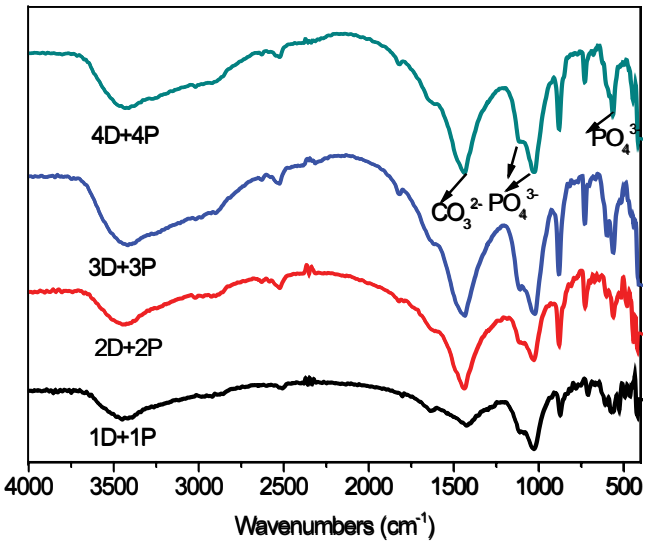

Fig. 1. FTIR of HAp-coated-limestone (1D + 1P, 2D + 2P, 3D + 3P, 4D + 4P).

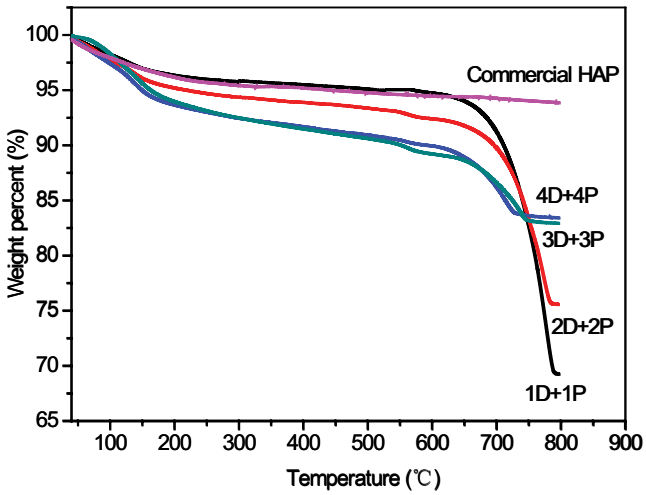

Fig. 2. TGA of five samples (commercial HAp, 1D + 1P, 2D + 2P, 3D + 3P, 4D + 4P).

(2) 180°C to 600°C, corresponding to the decomposition of HPO_4^{2-} according to the reaction:

$$HPO_4^{2-} \rightarrow P_2O_7^{4-} + H_2O \quad (3)$$

(3) At 600°C to 800°C, the weight loss of HAp-coated-limestone samples decreased rapidly. The fact is that limestone will decompose into calcium oxide and carbon dioxide. In addition, the less the addition amount of phosphate is, the faster the quality declines because the less the addition amounts of phosphate are, the less HAp onto the coverage is.

The XRD patterns of the synthetic phosphate coatings on granular limestone are transformed into HAp (Fig. 3). The primary region for the identification of the mineral form of apatite is 30.5°–34.5° 2θ [21]. $CaCO_3$ has peaks at 29.3°, 31.35°, 36.2°, 39.6° and 43.3°, whereas HAp has peaks at 32.2° and 34.1° 2θ. Peaks intensity of HAp gradually changed with the addition of phosphate, while peaks intensity of $CaCO_3$ weakened. Other calcium phosphate phases such as mono-, di-, tri- and octacalcium phosphates and their hydrated phases are not detected in the XRD patterns because powder XRD is a technique with low analytical limit. This observation of the presence of HAp suggests that HAp is the stable Ca-phosphate phase to form under the conditions in this study. From the analysis of the spectroscopic results, it was shown that the crystallographic characteristics of product were changed with phosphate addition times. Fast reaction of the crystals and ageing during preparation affected the crystal form and therefore the total surface area. For this, the specific surface area of HAp-coated-limestone was calculated with BET method (Table 2). It can be seen that the specific surface increased with the increasing of phosphate addition times. Therefore, both crystal form and coverage of HAp onto limestone affect the specific surface of HAp-coated-limestone.

The SEM images of unreacted limestone exhibit smoother surfaces than that of the phosphate reacted limestone (Fig. 4), and the morphology of precipitated HAp crystals changed with the growth conditions. The surface coverage increases continuously with the addition times of phosphate. However, complete coverage could not be achieved on all grains even after four phosphate additions.

3.2. Effect of phosphate addition times for adsorption

The adsorption capacity of HAp-coated-limestone on adsorption equilibrium at 60 min is shown in Fig. 5. It can be seen that the adsorption capacity of HAp-coated-limestone

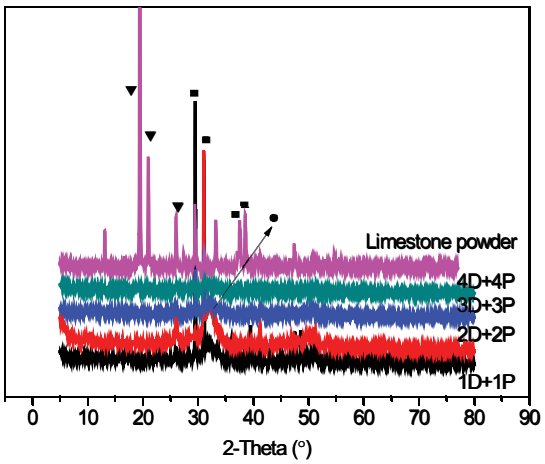

Fig. 3. XRD images of HAp-coated-limestone (■: $CaCO_3$, ▼: $Ca_5(PO_4)_3(OH)$, ●: SiO_2).

is gradually increasing with the increase of phosphate addition times. The adsorption capacity of HAp-coated-limestone which is obtained in a certain day (1, 2, 3 and 4 d) is 68.6, 72.1, 83.5 and 92.4 mg/g, respectively. The change of the HAp-coated-limestone removal efficiency with increasing phosphate addition times was attributed to the available surface area and adsorption sites. While under the same conditions, the commercial HAp is only 28.8 mg/g.

3.3. Adsorption kinetics

In order to explore the mechanism of the adsorption process of HAp-coated-limestone (4D + 4P) and obtain the equilibrium constant of adsorption and experiment data, we fit the model of pseudo-first-order adsorption kinetics and pseudo-second-order adsorption kinetics through the adsorption capacity over time. The pseudo-first-order adsorption kinetic model and the pseudo-second-order adsorption kinetic model is as below:

$$\log\left(Q_e - Q_t\right) = \log Q_e - \left(\frac{K_1}{2.303}\right)t \quad (4)$$

$$\frac{t}{Q_t} = \frac{1}{K_2 Q_e^2} + \frac{t}{Q_e} \quad (5)$$

In the formula, where Q_e (mg/g) is the amount of copper ions adsorbed in equilibrium, Q_e (mg/g) is the adsorption

Table 2
Textural properties of HA-coated-stones

Sample name	Textural properties		
	Pore volume ($cm^3\ g^{-1}$)	S_{BET} ($m^2\ g^{-1}$)	Average pore diameter (nm)
1D + 1P	0.116	35.7	29.3
2D + 2P	0.158	41.1	34.0
3D + 3P	0.150	39.07	31.4
4D + 4P	0.175	46.8	26.4

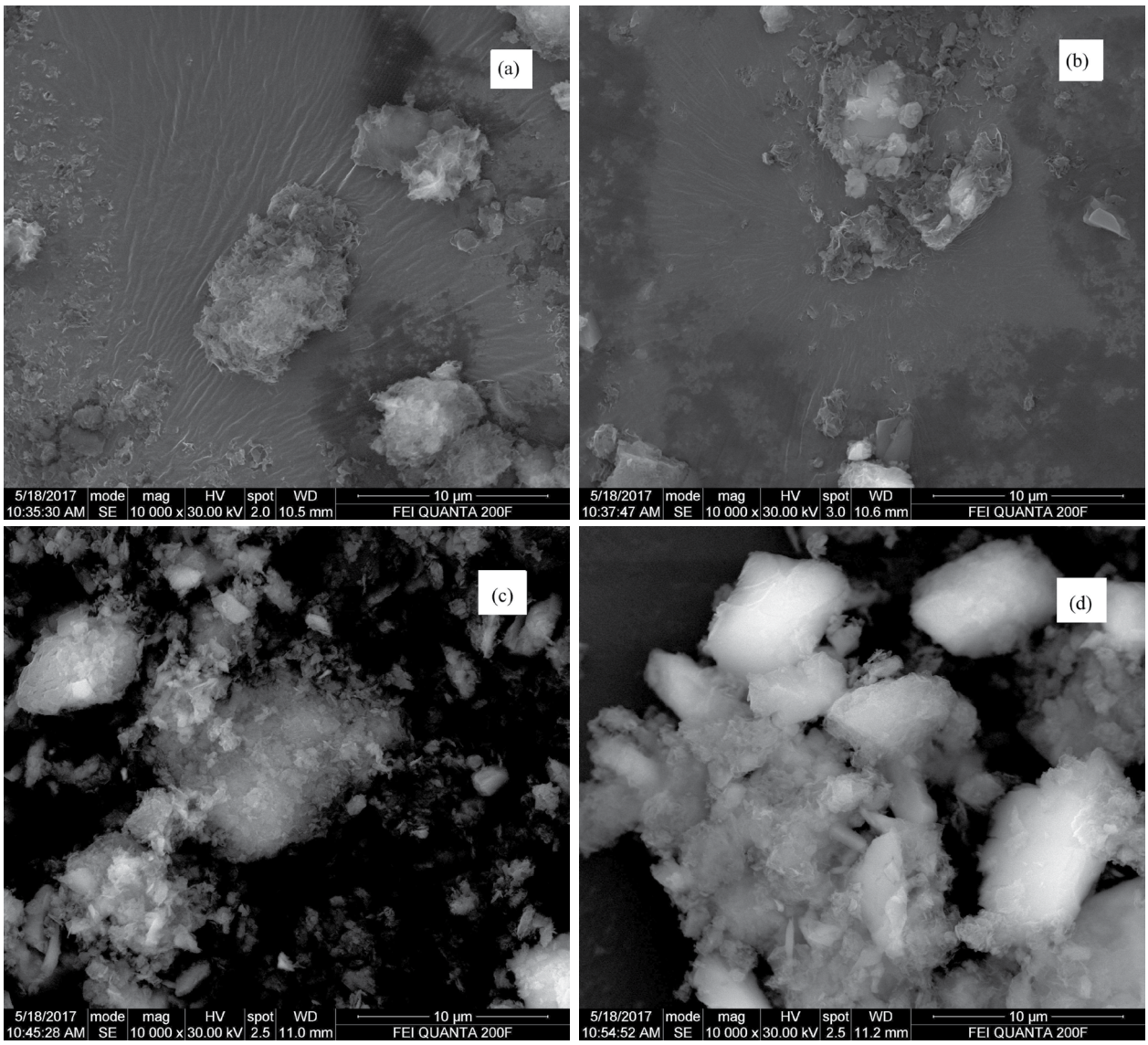

Fig. 4. SEM images of HAp-coated-limestone (a) 1D + 1P, (b) 2D + 2P, (c) 3D + 3P, and (d) 4D + 4P.

capacity at time t (min) and the value of K_1 (1/min) is the adsorption equilibrium constant of pseudo-first-order kinetics. K_2 (g/(mg min)) is the second-order kinetics constant. The adsorption kinetic parameters and the correlation coefficients (R^2) calculated from the functions of pseudo-first-order and pseudo-second-order kinetics that fitted in Fig. 6 are given in Table S1. It can be seen that in the pseudo-second-order kinetic model, the correlation coefficients (R^2) are closer to 0.999 or more than 0.999 than pseudo-first-order kinetic model. Therefore, the adsorption process is more consistent with the pseudo-second-order adsorption model rather than the pseudo-first-order kinetic model. In addition, according to Table S1, the Q_e obtained by the pseudo-second-order kinetic model is closer to the experimental data. Pseudo-second-order kinetics also better fit the experimental data. Based on these factors and data, pseudo-second-order adsorption kinetics is very suitable for HAp-coated-limestone adsorption on copper ions.

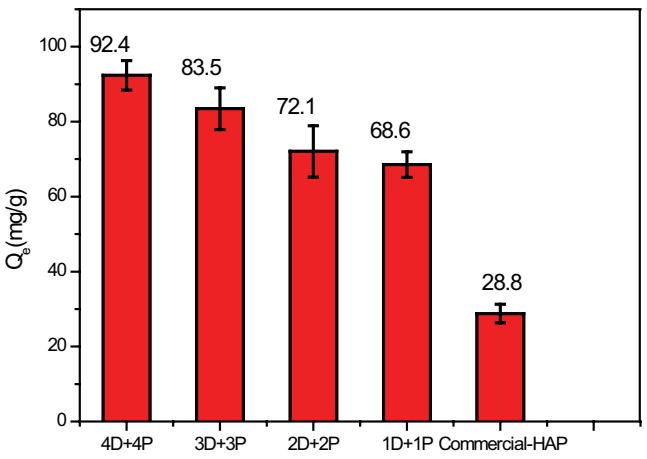

Fig. 5. Adsorption ability of Cu(II) by (commercial HAp, 1D + 1P, 2D + 2P, 3D + 3P, 4D + 4P) samples at 60 min.

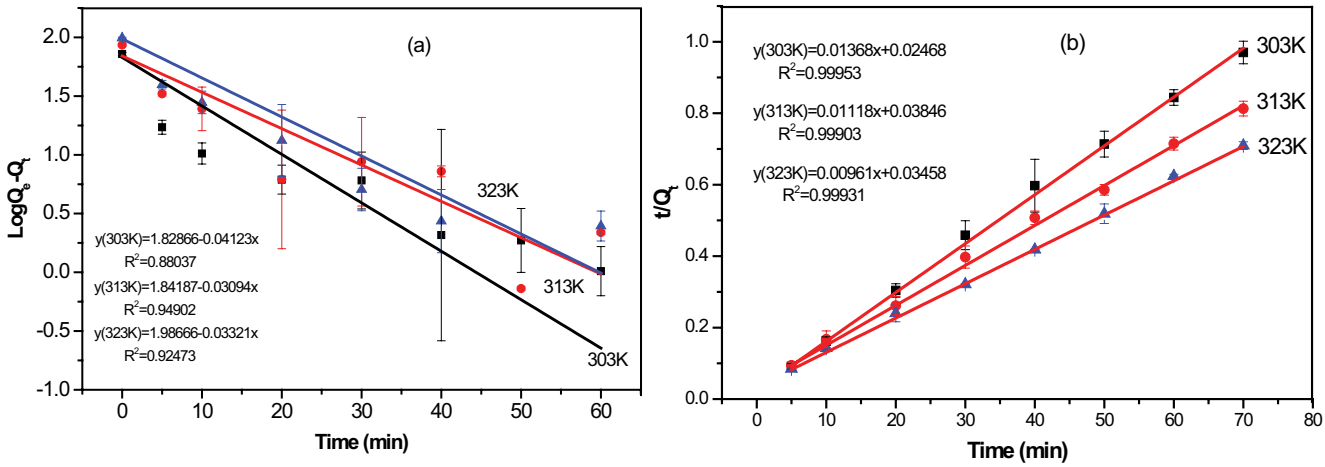

Fig. 6. Adsorption kinetic model for the adsorption of Cu(II) on the (4D + 4P) sample (a) pseudo-first-order and (b) pseudo-second-order.

The isotherms applicable to the adsorption of experimental data related to the Langmuir or Freundlich models. The linear form of the Langmuir model is expressed:

$$\frac{C_e}{Q_e} = \frac{1}{K_L Q_{\max}} + \frac{C_e}{Q_{\max}} \tag{6}$$

The linear form of the Freundlich model is expressed:

$$\log Q_e = \frac{1}{n}\log C_e + \log K_F \tag{7}$$

where C_e (mg/L) is the equilibrium concentration of Cu^{2+} ions, Q_e (mg/g) is the concentration of Cu^{2+} ions adsorbed by HAp-coated-limestone at equilibrium, K_L (L/mg) is the adsorption constant of Langmuir model and is relevant with energy, $Q_{\max}$ (mg/g) is the maximum adsorption capacity of HAp-coated-limestone, K_F is the Freundlich adsorption constant, and K_F and n are both related to adsorption capacity. The two models are fitted as Fig. 7. The values of two models' parameters are calculated by fitting the experimental data and the correlation coefficient. The adsorption isotherms of HAp-coated-limestone on Cu^{2+} conformed to Langmuir model, respectively, when the initial heavy metal ion concentration was 10–30 mg/L, the dosage of adsorbent was 10 mg, and the adsorption time was 60 min. And the adsorption temperatures are 303, 313 and 323 K. The isotherm parameter is obtained by subtracting the concentration range of the study by minimizing the sum of the squared error. And these parameters are listed as Table S2. It can be seen that the R^2 of all Langmuir isotherms are much larger than that of Freundlich, which means that the process of adsorbing of copper ions by HAp-coated-limestone conforms to the Langmuir model rather than the Freundlich model. Consistent with the Langmuir isotherms, it can be said that the adsorption of HAp-coated-limestone on copper ions is surface monolayer adsorption. And the adsorption capacity is related to the finite number of identified sites.

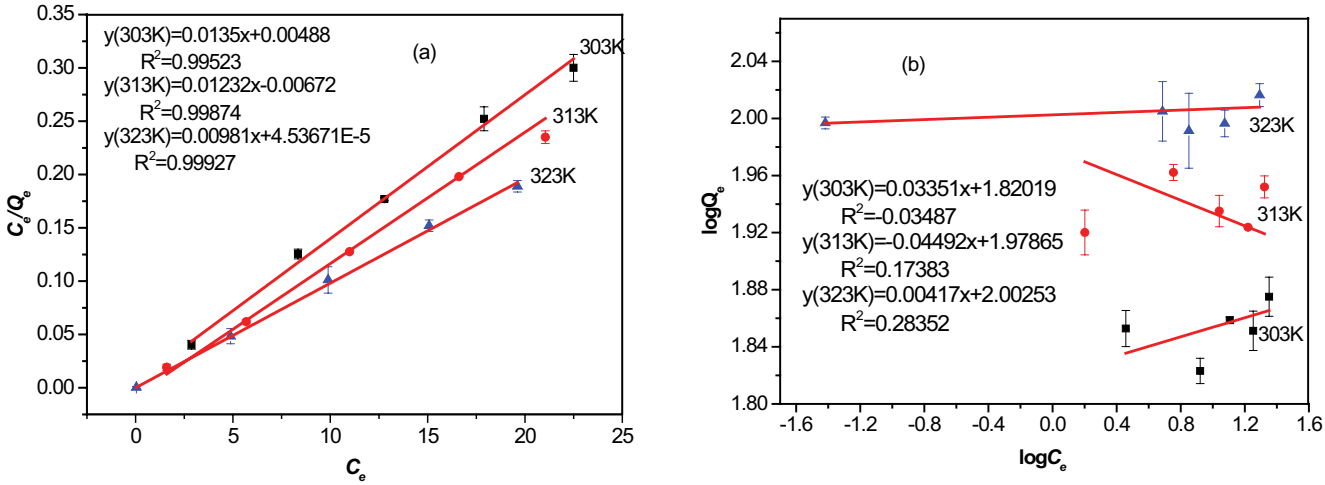

Fig. 7. (a) Langmuir and (b) Freundlich isotherm for the adsorption of Cu(II) on the (4D + 4P) sample.

In order to make sure whether the Langmuir model can well conform to the adsorption of HAp-coated-limestone on copper ions or not, R_L is used to indicate the correlation of the Langmuir model fit, and the meaning of R_L value is listed in Table S3. R_L is expressed as follows:

$$R_L = \frac{1}{1 + K_L C_0} \tag{8}$$

where C_0 is the initial concentration of copper ions, and K_L is the Langmuir constant.

3.4. Adsorption thermodynamics

In order to obtain the thermodynamic constants of the adsorption of copper ions by HA-coated-limestone, such as entropy change ($\Delta H°$), enthalpy change ($\Delta S°$), Gibbs free energy ($\Delta G°$), equations as follows are used to calculate: $K_a = \frac{Q_e}{C_e}$

$$\Delta G° = \Delta H° - T\Delta S° \tag{9}$$

$$\Delta G° = -RT\ln\left(55.5 \times K_a\right) \tag{10}$$

In the equations, where C_e (mg/L) is the concentration on adsorption equilibrium, Q_e (mg/g) is the adsorption capacity at equilibrium. T (K) is the temperature of copper ion solution that was used to adsorb, R is the gas constant (8.314 J/mol K), and K_a is the constant of equilibrium on adsorption process and the number 55.5 represents the amounts of moles of H_2O per liter of solution. In the figure, the natural logarithm of the negative equilibrium constant ($-\ln K_a$) is plotted against the reciprocal of the corresponding temperature ($1/T$) to obtain a straight line in Fig. 7. $\Delta H°$ can be calculated by the slope $\left(\text{slope} = \frac{\Delta H°}{R}\right)$, and $\Delta S°$ can be calculated by the intercept $\left(\text{intercept} = \frac{\Delta S°}{R}\right)$. These thermodynamic parameters are all listed in Table S4. The value of $\Delta H°$ is a positive number, and it is demonstrated that the adsorption process is endothermic, and the elevated temperature is favorable for adsorption. The value of $\Delta S°$ is greater than zero, which means that the adsorption is random and irreversible. As the temperature increases, the randomness and irreversibility of the adsorption process increase. $\Delta G°$ is positive, which indicates that the adsorption is spontaneous at this temperature. The temperature increased from 303.15 to 323.15 K, and $\Delta G°$ rose from –4.3 to –7.1 kJ moL^{-1}. All of these thermodynamic parameters show that HAp-coated-limestone is effective to adsorb copper ions in the process.

3.5. Effect of solution pH on adsorption

The solution pH is an important parameter influencing the sorption process at the water–sorbent interfaces. To determine the optimum removal pH of Cu(II), the equilibrium sorption of Cu(II) was investigated over a pH range of 2–7. pH value greatly affected the adsorption of Cu(II) on sample 4D + 4P. At higher pH values, Cu(II) ions precipitate as hydroxides. As is illustrated in Fig. 8a, the adsorption capacity at pH 2.0 was zero. The reason may be that the structure of HAp-coated-limestone was destroyed. And there was a dramatic increase of adsorption capacity as the pH increased from 3.0 to 7.0. The removal efficiency of Cu(II) was about 93.8 mg/g at pH 7.0 and only 21.4 mg/g at pH 3.0. This adsorption process could be expressed as the following reaction equation:

$$\text{HAp-}\left(\text{OH}\right)_2 + \text{Cu}^{2+} \Leftrightarrow \text{HAp} - \text{O}_2 - \text{Cu}^{2+} + 2\text{H}^+ \tag{11}$$

It can be seen that the higher the pH value is, the lower the concentration of hydrogen ions is. Hence, the reaction was carried out in the direction of adsorbing copper ions and the adsorption capacity increased. The optimum pH for adsorbing Cu(II) ion is found in the pH range of 5–7 which is in accordance with previous reports [29–32].

It can be seen (Fig. 8b) that the 4D + 4P has the buffering properties. The final pH was alkaline regardless of the initial pH range 2–7. The buffering characteristics of sample 4D + 4P resulted in the acid–base reactions of the reactive surface sites. The reactions responsible for the surface properties of sample 4D + 4P in aqueous solutions are [33] as follows:

$$\equiv \text{PO}^- + \text{H}^+ \leftrightarrow \equiv \text{PHO}° \tag{12}$$

$$\equiv \text{CaOH}_2^+ \leftrightarrow \equiv \text{CaOH}° + \text{H}^+ \tag{13}$$

In the acidic environment, there is a positive shift in the final solution pH relative to initial pH value after 120 min of adsorption according to Fig. 8b. The pH shift may be the fact that limestone reacts with acid material.

3.6. Influence of ions on Cu^{2+} sorption

Inorganic salts are always in the wastewater. As electrostatic interaction played a crucial role in the adsorption of Cu^{2+} on the sample 4D + 4P, these inorganic salts in wastewater may affect the adsorption process by competing for the charged sites on its surface. Therefore, it is necessary to study the influence of inorganic salts on the adsorption performance of the sample 4D + 4P. The influence of Mg^{2+} on the adsorption of MB on the sample 4D + 4P was presented in Fig. 9a. It was found that, as the concentration of Mg^{2+} increased, the adsorbed Cu^{2+} decreased. These results demonstrated that the presence of Mg^{2+} inhibited the adsorption of Cu^{2+}, and the inhibiting effect became stronger with the ionic strength increased. The main reason was that there was a competitive adsorption between salt ions and Cu^{2+} on the surface of the sample 4D + 4P, that is, some salt ions occupied a certain amount of adsorption sites, leading to a decrease in the adsorption sites of Cu^{2+}. Additionally, the influence of co-anions, such as NO_3^-, SO_4^{2-} and Cl^-, on the adsorption of Cu^{2+} by the sample 4D + 4P was studied. As shown in Fig. 9b, it was found that the presence of NO_3^-, SO_4^{2-} and Cl^- also inhibited the adsorption capacity of the Cu^{2+}.

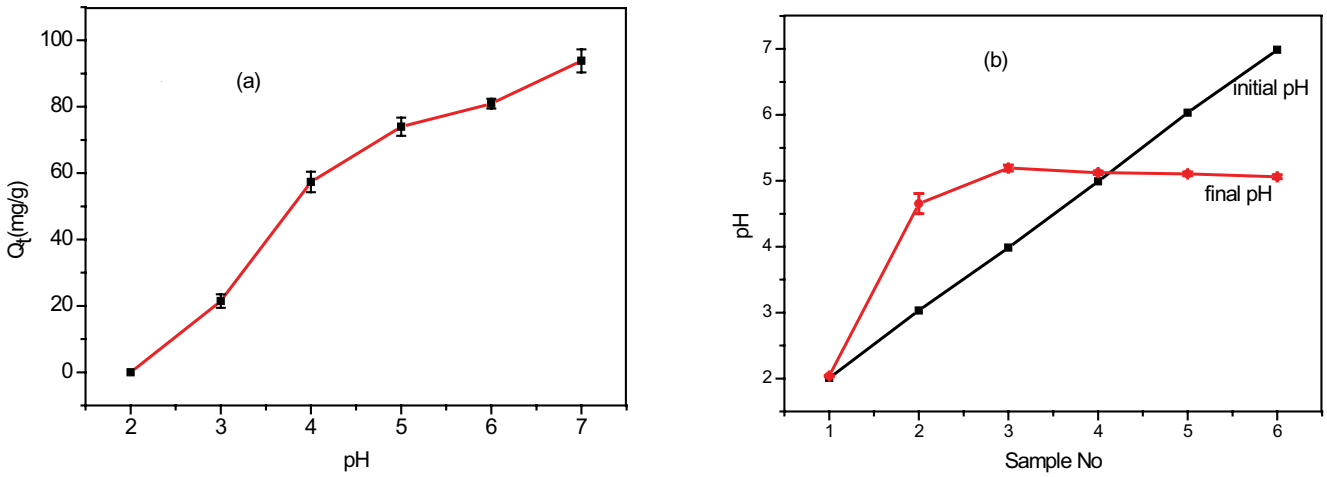

Fig. 8. (a) Effect of initial pH for Cu(II) adsorption and (b) pH values before and after adsorption.

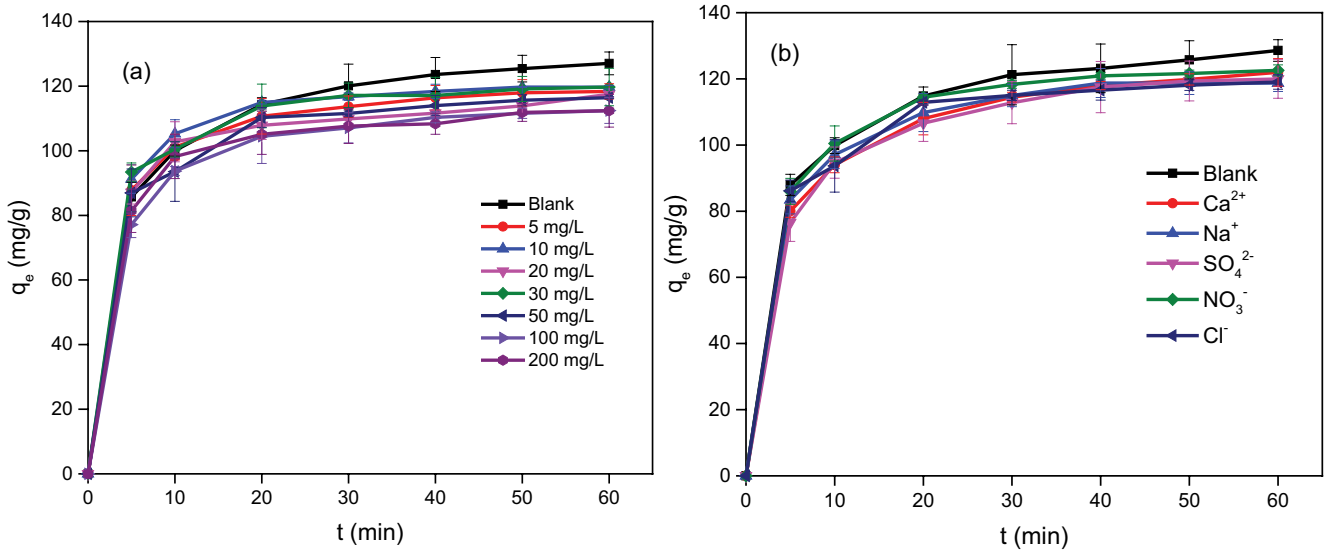

Fig. 9. (a) Effect of Mg^{2+} with different concentrations and (b) influence of ions on Cu^{2+} sorption.

3.7. Mechanisms of Cu(II) adsorption onto HAp-coated-limestone surface

According to the previous studies [34–37], the possible mechanisms for Cu(II) retention by HAp-coated-limestone included (1) ion exchange with Ca^{2+} of HAp (HAp-Ca^{2+} + Cu^{2+}→HAp-Cu^{2+} + HAp-Ca^{2+}); (2) surface complexation of Cu(II) on the ≡P–OH groups of HAp [HAp-OH + Cu^{2+} = HAp-O-Cu^{+} + H^{+} or HAp-$(OH)_2$ + Cu^{2+} = HAp-O_2-Cu^{2+} + $2H^{+}$]. (3) dissolution of HAp followed by the precipitation of Cu-containing HAp with formula $Cu_xCa_{10-x}(PO_4)_6(OH)_2$. It was considered that the limestone can provide additional substrate for the surface of HAp, as a result, was enhanced adsorption of Cu(II) ions. Fig. S1 shows the SEM–EDX image of HAp-coated-limestone after adsorption. The amount of Cu on the surface of HA-coated-limestone increased with the increase of phosphate addition times. The amounts of Cu were 6.35% for 1D + 1P, while the amounts of sulfur were 7.59% for 4D + 4P. The possible mechanisms for Cu(II) adsorption onto HAp-coated-limestone surface have been presented in Fig. 10.

3.8. Comparison with other adsorbents

HAp was mostly prepared through hydrothermal method at high temperature heating, with calcium nitrate as raw material [38]. The reaction conditions are relatively harsh. However, in this study, HAp-coated-limestone was prepared with waste limestone and dihydrogen phosphate diamine, which was low in cost and did not require harsh preparation conditions, and samples were obtained only by reaction at a typical temperature for several days. In addition, the solution temperature is 303 K, the adsorption capacity of HAp-coated-limestone on copper ions is 72.2 mg/g, which is much larger than that of the modified hydroxyapatite. Compared with other adsorbents listed as Table S5, the adsorption capacity and efficiency are higher, and the cost is lower.

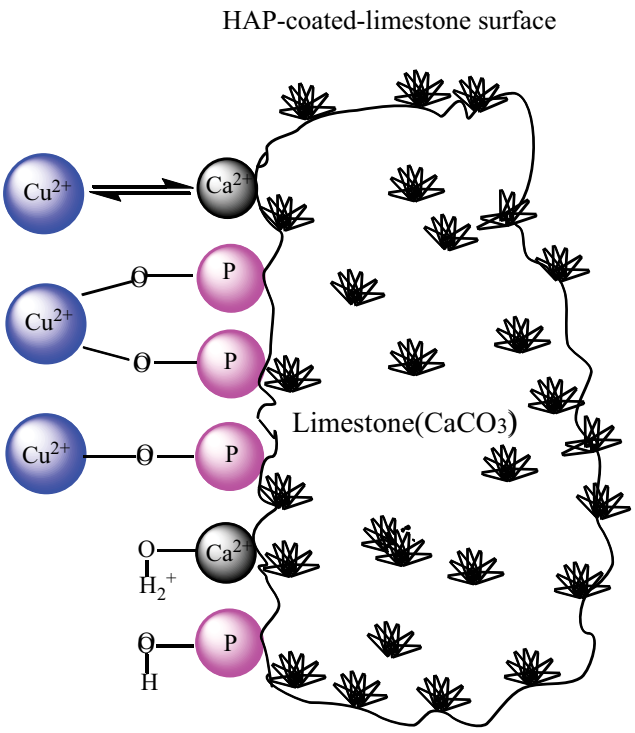

Fig. 10. Possible mechanisms for Cu(II) adsorption onto HAp-coated-limestone surface.

All the comparisons between HAp-coated-limestone and other adsorption are listed below.

4. Conclusion

HAp-coated-limestone was successfully prepared using limestone and diammonium hydrogen phosphate and its adsorption capacity was superior to that of commercial nano-hydroxyapatite. The process of adsorbing copper ions is spontaneous, irreversible and endothermic. The adsorption of copper ions on the sample is more consistent with the Langmuir isotherm. The second-order kinetics can better fit the adsorption process of HAp-coated-limestone. The adsorption capacity of HAp-coated-limestone is gradually increasing with the increase of phosphate addition times. The adsorption capacity of HAp-coated-limestone (1D + 1P, 2D + 2P, 3D + 3P, 4D + 4P) is 68.6, 72.1, 83.5 and 92.4 mg/g at 60 min, respectively. Both crystal form and HAp onto the coverage of limestone affect the specific surface of HAp-coated-limestone. The advantages of HAp-coated-limestone prepared in this experiment are that the easy copolymerization problem of nano-hydroxyapatite has been solved and the adsorption capacity has not been reduced but greatly increased.

Acknowledgments

The work was supported by State Key Laboratory of Pollution Control and Resource Reuse open foundation for financial support under research projects PCRRF11018, and Foundation of the Creative Experimental Project of National undergraduate students for financial support under research projects 20140403029.

References

[1] O. Rosskopfová, M. Galamboš, J. Ometáková, M. Čaplovičová, P. Rajec, Study of sorption processes of copper on synthetic hydroxyapatite, J. Radioanal. Nucl. Chem., 293 (2012) 641–647.
[2] R. Foroutan, R. Mohammadi, S. Farjadfard, H. Esmaeili, M. Saberi, S. Sahebi, S. Dobaradaran, B. Ramavandi, Characteristics and performance of Cd, Ni, and Pb bio-adsorption using *Callinectes sapidus* biomass: real wastewater treatment, Environ. Sci. Pollut. Res., 26 (2019) 6336–6347.
[3] K. Page, M.J. Harbottle, P.J. Cleall, T.R. Hutchings, Heavy metal leaching and environmental risk from the use of compost-like output as an energy crop growth substrate, Sci. Total Environ., 487 (2014) 260–271.
[4] C.Y. Chang, H.Y. Yu, J.J. Chen, F.B. Li, H.H. Zhang, C.P. Liu, Accumulation of heavy metals in leaf vegetables from agricultural soils and associated potential health risks in the Pearl River Delta, South China, Environ. Monit. Assess., 186 (2014) 1547–1560.
[5] M.A.H. Bhuiyan, M.A. Islam, S.B. Dampare, L. Parvez, S. Suzuki, Evaluation of hazardous metal pollution in irrigation and drinking water systems in the vicinity of a coal mine area of northwestern Bangladesh, J. Hazard. Mater., 179 (2010) 1065–1077.
[6] F.-M. Pellera, A. Giannis, D. Kalderis, K. Anastasiadou, R. Stegmann, J.-Y. Wang, E. Gidarakos, Adsorption of Cu(II) ions from aqueous solutions on biochars prepared from agricultural by-products, J. Environ. Manage., 96 (2012) 35–42.
[7] S.A. Al-Saydeh, M.H. El-Naas, S.J. Zaidi, Copper removal from industrial wastewater: a comprehensive review, J. Ind. Eng. Chem., 56 (2017) 35–44.
[8] Y.-c. Lin, H.-p. Wang, F. Gohar, M.H. Ullah, X. Zhang, D.-f. Xie, H. Fang, J. Huang, J.-x. Yang, Preparation and copper ions adsorption properties of thiosemicarbazide chitosan from squid pens, Int. J. Biol. Macromol., 95 (2017) 476–483.
[9] A. Pal, J. Jayamani, R. Prasad, An urgent need to reassess the safe levels of copper in the drinking water: lessons from studies on healthy animals harboring no genetic deficits, Neuro Toxicology, 44 (2014) 58–60.
[10] F. Fu, Q. Wang, Removal of heavy metal ions from wastewaters: a review, J. Environ. Manage., 92 (2011) 407–418.
[11] H. Kokes, M.H. Morcali, E. Acma, Dissolution of copper and iron from malachite ore and precipitation of copper sulfate pentahydrate by chemical process, Eng. Sci. Technol., 17 (2014) 39–44.
[12] Y. Wei, Q. Zhang, W.-J. Wang, B.-G. Li, S. Zhu, Improvement on stability of polymeric latexes prepared by emulsion ATRP through copper removal using electrolysis, Polymer, 106 (2016) 261–266.
[13] X. Xie, R. Deng, Y. Pang, Y. Bai, W. Zheng, Y. Zhou, Adsorption of copper(II) by sulfur microparticles, Chem. Eng. J., 314 (2017) 434–442.
[14] V.K. Gupta, P. Singh, N. Rahman, Adsorption behavior of Hg(II), Pb(II), and Cd(II) from aqueous solution on Duolite C-433: a synthetic resin, J. Colloid Interface Sci., 275 (2004) 398–402.
[15] W.-Q. Tang, R.-Y. Zeng, Y.-L. Feng, X.-M. Li, W. Zhen, Removal of Cr(VI) from aqueous solution by nano-carbonate hydroxylapatite of different Ca/P molar ratios, Chem. Eng. J., 223 (2013) 340–346.
[16] H. Demiral, C. Güngör, Adsorption of copper(II) from aqueous solutions on activated carbon prepared from grape bagasse, J. Cleaner Prod., 124 (2016) 103–113.
[17] X. Zhang, Q. Huang, M. Liu, J. Tian, G. Zeng, Z. Li, K. Wang, Q. Zhang, Q. Wan, F. Deng, Y. Wei, Preparation of amine functionalized carbon nanotubes via a bioinspired strategy and their application in Cu^{2+} removal, Appl. Surf. Sci., 343 (2015) 19–27.
[18] R. Bazargan-Lari, H.R. Zafarani, M.E. Bahrololoom, A. Nemati, Removal of Cu(II) ions from aqueous solutions by low-cost

natural hydroxyapatite/chitosan composite: equilibrium, kinetic and thermodynamic studies, J. Taiwan Inst. Chem. Eng., 45 (2014) 1642–1648.
[19] N.N. Seda, F. Koenigsmark, T.M. Vadas, Sorption and coprecipitation of copper to ferrihydrite and humic acid organomineral complexes and controls on copper availability, Chemosphere, 147 (2016) 272–278.
[20] D. Kanakaraju, S. Ravichandar, Y.C. Lim, Combined effects of adsorption and photocatalysis by hybrid TiO_2/ZnO-calcium alginate beads for the removal of copper, J. Environ. Sci., 55 (2017) 214–223.
[21] A. Szcześ, L. Hołysz, E. Chibowski, Synthesis of hydroxyapatite for biomedical applications, Adv. Colloid Interface Sci., 249 (2017) 321–330.
[22] O. Bareiro, L.A. Santos, Tetraethylorthosilicate (TEOS) applied in the surface modification of hydroxyapatite to develop polydimethylsiloxane/hydroxyapatite composites, Colloids Surf., B, 115 (2014) 400–405.
[23] M.S. Fernando, R.M. de Silva, K.M.N. de Silva, Synthesis, characterization, and application of nano hydroxyapatite and nanocomposite of hydroxyapatite with granular activated carbon for the removal of Pb^{2+} from aqueous solutions, Appl. Surf. Sci., 351 (2015) 95–103.
[24] C.M. Kanno, R.L. Sanders, S.M. Flynn, G. Lessard, S.C.B. Myneni, Novel apatite-based sorbent for defluoridation: synthesis and sorption characteristics of nano-micro-crystalline hydroxyapatite-coated-limestone, Environ. Sci. Technol., 48 (2014) 5798–5807.
[25] F. Xu, C. Jiang, D. Li, Defluoridation of wastewaters using HAP-coated-limestone, Sep. Sci. Technol., (2018), doi: https://doi.org/10.1080/01496395.2018.1541470.
[26] M. Kamiya, J. Hatta, E. Shimada, Y. Ikuma, M. Yoshimura, H. Monma, AFM analysis of initial stage of reaction between calcite and phosphate, Mater. Sci. Eng., B, 111 (2004) 226–231.
[27] M.A. Osman, U.W. Suter, Surface treatment of calcite with fatty acids: structure and properties of the organic monolayer, Chem. Mater., 14 (2002) 4408–4415.
[28] K. Shiba, S. Motozuka, T. Yamaguchi, N. Ogawa, Y. Otsuka, K. Ohnuma, T. Kataoka, M. Tagaya, Effect of cationic surfactant micelles on hydroxyapatite nanocrystal formation: an investigation into the inorganic–organic interfacial interactions, Cryst. Growth Des., 16 (2016) 1463–1471.
[29] X.S. Wang, L. Zhu, H.J. Lu, Surface chemical properties and adsorption of Cu (II) on nanoscale magnetite in aqueous solutions, Desalination, 276 (2011) 154–160.
[30] X. Xin, Q. Wei, J. Yang, L. Yan, R. Feng, G. Chen, B. Du, H. Li, Highly efficient removal of heavy metal ions by amine-functionalized mesoporous Fe_3O_4 nanoparticles, Chem. Eng. J., 184 (2012) 132–140.
[31] X. Peng, Z. Luan, Z. Di, Z. Zhang, C. Zhu, Carbon nanotubes-iron oxides magnetic composites as adsorbent for removal of Pb(II) and Cu(II) from water, Carbon, 43 (2005) 880–883.
[32] Y. Liu, M. Chen, H. Yongmei, Study on the adsorption of Cu(II) by EDTA functionalized Fe_3O_4 magnetic nano-particles, Chem. Eng. J., 218 (2013) 46–54.
[33] S. Hokkanen, A. Bhatnagar, E. Repo, S. Lou, M. Sillanpää, Calcium hydroxyapatite microfibrillated cellulose composite as a potential adsorbent for the removal of Cr(VI) from aqueous solution, Chem. Eng. J., 283 (2016) 445–452.
[34] Y. Zhan, J. Lin, J. Li, Preparation and characterization of surfactant-modified hydroxyapatite/zeolite composite and its adsorption behavior toward humic acid and copper(II), Environ. Sci. Pollut. Res. Int., 20 (2013) 2512–2526.
[35] F. Fernane, M.O. Mecherri, P. Sharrock, M. Hadioui, H. Lounici, M. Fedoroff, Sorption of cadmium and copper ions on natural and synthetic hydroxylapatite particles, Mater. Charact., 59 (2008) 554–559.
[36] Y.-J. Wang, J.-H. Chen, Y.-X. Cui, S.-Q. Wang, D.-M. Zhou, Effects of low-molecular-weight organic acids on Cu(II) adsorption onto hydroxyapatite nanoparticles, J. Hazard. Mater., 162 (2009) 1135–1140.
[37] L. Yang, W. Zhong, J. Cui, Z. Wei, W. Wei, Enhanced removal of Cu(II) ions from aqueous solution by poorly crystalline hydroxyapatite nanoparticles, J. Dispersion Sci. Technol., 37 (2016) 956–968.
[38] A. Fihri, C. Len, R.S. Varma, A. Solhy, Hydroxyapatite: a review of syntheses, structure and applications in heterogeneous catalysis, Coord. Chem. Rev., 347 (2017) 48–76.
[39] G.M. Rajiv, G.N. Kousalya, S. Meenakshi, Removal of copper(II) using chitin/chitosan nano-hydroxyapatite composite, Int. J. Biol. Macromol., 48 (2011) 119–124.
[40] B. Al-Rashdi, C. Tizaoui, N. Hilal, Copper removal from aqueous solutions using nano-scale diboron trioxide/titanium dioxide (B_2O_3/TiO_2) adsorbent, Chem. Eng. J., 183 (2012) 294–302.
[41] Y.-H. Chen, F.-A. Li, Kinetic study on removal of copper(II) using goethite and hematite nano-photocatalysts, J. Colloid Interface Sci., 347 (2010) 277–281.
[42] M.M. Rao, D.K. Ramana, K. Seshaiah, M.C. Wang, S.W.C. Chien, Removal of some metal ions by activated carbon prepared from *Phaseolus aureus* hulls, J. Hazard. Mater., 166 (2009) 1006–1013.
[43] C.-H. Wu, Studies of the equilibrium and thermodynamics of the adsorption of Cu^{2+} onto as-produced and modified carbon nanotubes, J. Colloid Interface Sci., 311 (2007) 338–346.
[44] P. Sricharoen, N. Limchoowong, Y. Areerob, P. Nuengmatcha, S. Techawongstien, S. Chanthai, Fe_3O_4/hydroxyapatite/graphene quantum dots as a novel nano-sorbent for preconcentration of copper residue in Thai food ingredients: optimization of ultrasound-assisted magnetic solid phase extraction, Ultrason. Sonochem., 37 (2017) 83–93.
[45] A.L. da Silva Lage Moreira, A. de Souza Pereira, M.G. Speziali, K.M. Novack, L.V. Alves Gurgel, L.F. Gil, Bifunctionalized chitosan: a versatile adsorbent for removal of Cu(II) and Cr(VI) from aqueous solution, Carbohydr. Polym., 201 (2018) 218–227.
[46] J. Wang, S. Zheng, Y. Shao, J. Liu, Z. Xu, D. Zhu, Amino-functionalized Fe_3O_4@SiO_2 core–shell magnetic nanomaterial as a novel adsorbent for aqueous heavy metals removal, J. Colloid Interface Sci., 349 (2010) 293–299.
[47] H. Faghihian, Z. Adibmehr, Comparative performance of novel magnetic ion-imprinted adsorbents employed for Cd^{2+}, Cu^{2+} and Ni^{2+} removal from aqueous solutions, Environ. Sci. Pollut. Res., 25 (2018) 15068–15079.

Supplementary Information

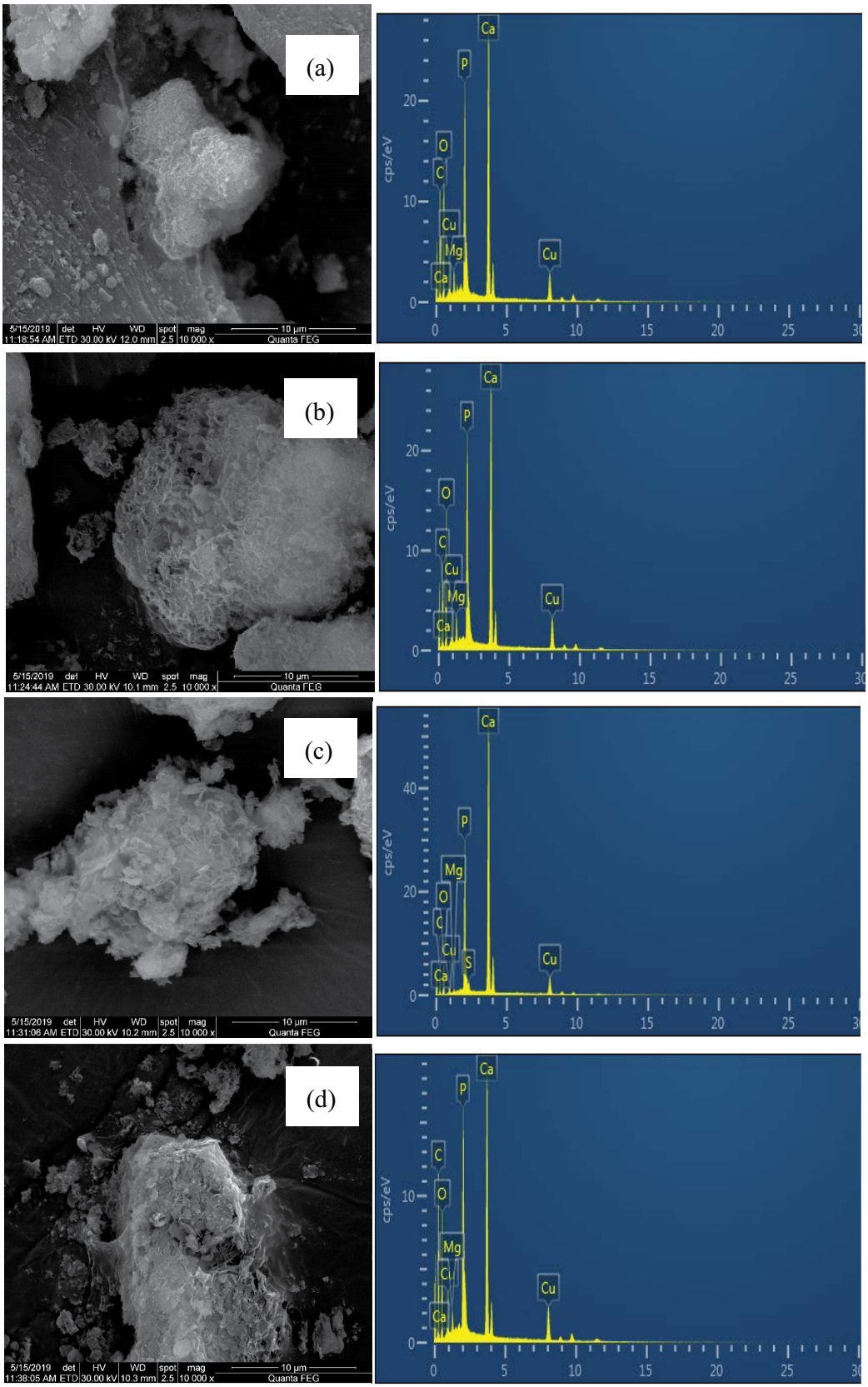

Fig. S1. SEM–EDX image of HAp-coated-limestone after adsorption (a) 1D + 1P, (b) 2D + 2P, (c) 3D + 3P and (d) 4D + 4P.

Table S1
Adsorption kinetic parameters for Cu(II) by HAp-coated-limestone (4D + 4P)

Temperature (K)	Experimental Q_e (mg g^{-1})	Pseudo-first-order			Pseudo-second-order		
		K_1	Q_e (mg g^{-1})	R^2	K_2	Q_e (mg g^{-1})	R^2
303	72.2	0.04123	67.4	0.88037	0.007583	73.1	0.99953
313	86.1	0.03094	69.5	0.94902	0.00325	89.4	0.99903
323	98.7	0.03321	97.0	0.92473	0.002671	104.0	0.99931

Table S2
Parameters of adsorption of Cu(II) on HAp-coated-limestone (4D + 4P) at different temperatures

S. No	Temperature (K)	Langmuir adsorption isotherm			Freundlich adsorption isotherm		
		Q_{max} (mg/g)	K_L (L/mg)	R^2	1/n	K_F	R^2
1	303	74.1	2.77	0.9952	0.0335	66.098	–0.0349
2	313	81.2	–1.83	0.9987	0.0449	95.203	0.1738
3	323	101.9	216.24	0.9993	0.0042	100.584	0.2835

Table S3
Value of R_L indicates the shape of the Langmuir isotherm

Value of R_L	Type of isotherm
$R_L > 1$	Unfavorable
$R_L = 1$	Linear
$0 < R_L < 1$	Favorable
$R_L < 0$	Irreversible

Table S4
Data of the thermodynamic parameters for the adsorption of Cu(II) on HAp-coated-limestone (4D + 4P)

S. No	Temperature (K)	$\Delta G°$ (kJ/mol)	$\Delta H°$ (kJ/mol)	$\Delta S°$ (J/mol K)
1	303	–14.48	91.48	359.30
2	313	–15.61		
3	323	–16.99		

Table S5
Comparison of adsorption capacity of several adsorbents for Cu(II)

Absorbent	Capacity (mg/g)	References
HAp-coated-limestone	74.07	This study
EDTA-functionalized magnetic nanoparticles	46.27	[32]
Synthetic HAp	30.5	[37]
HAp-nanoparticles	29.23	[1]
Humic acid modified HAp nanoparticles	58.42	[19]
Nano-hydroxyapatite/chitin composite	21.45	[39]
Nano-B_2O_3/TiO_2	82	[40]
Nano-goethite	149.25	[41]
CNTs-PDA-PP	26.4	[17]
Activated carbon	19.50	[42]
As-produced CNTs	8.25	[43]
Fe_3O_4/hydroxyapatite/graphene	41.9	[44]
Bifunctionalized chitosan	165.2	[45]
Amino-functionalized Fe_3O_4@SiO_2 magnetic nanomaterial	43.85	[46]
Cu(II)-MIIP	95	[47]